

FREQUENCY-BIN GEOMETRIC ALGEBRA FOR STRUCTURED AND RELATIONAL INFORMATION: ENCODING METHODS AND APPLICATIONS

M. Svítek[*]

Abstract: This paper develops the implementation and application layer of Frequency-Bin Geometric Algebra (FB-GA) once the underlying blade structure has been specified. The framework combines symbolic construction of sparse multivectors with collision-free spectral encoding and reciprocal extraction of accepted blades from measured channels. Beyond grade-specific vector, bivector, trivector, and higher-grade coefficients, the application perspective is extended to structured relations among grade sectors, enabling the definition of multigrade relational fingerprints. A Beijing environmental data set provides realistic nonstationary signals for an encoding demonstration and illustrates how such relational descriptors can be constructed after blade reconstruction. A second example uses frequency-bin convolution, selected joint channels, and opposite complex rotations to generate quantum-like coefficient patterns, including Bell-like non-factorizable states. The neural and cognitive interpretation is then extended toward Spatiotemporal Geometry Integration Theory (SGIT), where spatiotemporal multigrade relational geometry is proposed as a future framework for identifying reproducible patterns of integration. The emphasis throughout is operational: how structured geometric-algebra information can be encoded, reconstructed, compared, and interpreted across different application domains.

Key words: *geometric algebra, frequency-bin encoding, signal synthesis, multivectors, quantum-like information processing, multigrade relational geometry, Spatiotemporal Geometry Integration Theory, neuroinformatics*

Received: January 20, 2026 **DOI:** 10.14311/NNW.2026.36.004
Revised and accepted: April 25, 2026

1. Introduction

A frequency-domain implementation becomes useful when an algebraic object must be transported, synthesized, or reconstructed through signal-processing hardware or software. Frequency-bin technologies already provide controllable spectral modes with complex amplitudes [1, 2]; geometric algebra provides the blade structure that

[*]Miroslav Svítek; Czech Technical University in Prague, Faculty of Transportation Sciences, Czech Republic; Matej Bel University in Banská Bystrica, Slovakia

©CTU FTS 2026

specifies how elementary components and their relations are organized [3, 4]. The practical question addressed here is how these two layers can be connected without confusing a physical mixing product with a geometric operation.

The companion theoretical paper defines the FB-GA hierarchy, including sparse support, orientation, exterior composition, relational objects, and relations among structures of different grades [21]. The emphasis of this paper is different: a blade dictionary is first constructed, each active blade is mapped to a prescribed spectral signature, and the receiver accepts a reconstructed blade only when the complete address pattern satisfies the decoding rule. A second analytical layer can then operate on the accepted blades themselves. In that layer, the information of interest is not only which vectors, bivectors, trivectors, or higher-grade blades are present, but also how structures belonging to different grades are mutually organized.

This distinction is important for applications. Conventional spectral modulation primarily addresses how numerical coefficients are carried. FB-GA can additionally preserve grade, orientation, blade identity, and a relational architecture among the reconstructed components. The resulting object is therefore not merely a collection of modulated spectral channels; it can be treated as a structured multigrade representation whose internal relations are available for further comparison, classification, or physical interpretation.

Three application-oriented settings are considered. Measured Beijing series provide realistic envelopes for a waveform-encoding example and a transparent demonstration of multigrade organization. Frequency-bin convolution and polarization-sensitive selection illustrate classical quantum-like composition and Bell-like coefficient structures. Finally, the same encoding hierarchy is developed as an organizational language for neural and cognitive signals and as a bridge toward Spatiotemporal Geometry Integration Theory (SGIT).

2. Operational FB-GA Conventions

For implementation, an FB-GA object is treated first as a sparse collection of labelled blades with real or complex coefficients. Standard geometric-algebra notation is used [3, 4]: e_i denotes a basis vector, $e_{ij} = e_i \wedge e_j$ an oriented bivector, and $e_{ijk} = e_i \wedge e_j \wedge e_k$ a trivector. Reversing the order of independent basis directions changes the sign of the blade.

The relational layer records structured dependencies among already identified blades, including relations between different grades. Such an inter-grade relation does not necessarily mean that the two blades are exterior-multiplied. It may instead denote a reproducible dependence, correspondence, conditional association, phase organization, geometric alignment, or another domain-specific coupling between their coefficients, supports, or subspaces.

A vector coefficient can be carried by one complex frequency-bin channel,

$$s_i(t) = \mathrm{Re}\left\{C_i(t)\mathrm{e}^{\mathrm{i}2\pi f_i t}\right\}, \tag{1}$$

where $C_i(t)$ contains the in-phase and quadrature information and f_i is the assigned carrier address. Several vector channels can be added linearly without changing their algebraic grade.

For a measured real series $x_i(t)$, the analytic representation

$$z_i(t) = x_i(t) + \mathrm{i}\mathcal{H}\{x_i(t)\} \tag{2}$$

provides a convenient complex coefficient. One possible antisymmetric pair coefficient is then

$$B_{ij}(t) = \mathrm{Im}\{z_i(t)z_j^*(t)\}, \qquad B_{ji}(t) = -B_{ij}(t). \tag{3}$$

A third independent direction can extend an already identified pair,

$$\big(B_{ij}(t)e_{ij}\big) \wedge \big(C_k(t)e_k\big) = \eta_{ijk}B_{ij}(t)C_k(t)e_{ijk}, \qquad k \notin \{i,j\}, \tag{4}$$

where $\eta_{ijk} \in \{-1,+1\}$ restores the canonical index order. In the signal layer, one trivector is assigned a coherent multi-address signature; all of its required channels must be present and mutually compatible after known deterministic corrections.

The complete transmitted waveform is obtained by superposing the spectral signatures of all active blades,

$$s_{\mathrm{FB-GA}}(t) = s_V(t) + s_B(t) + s_T(t) + \cdots . \tag{5}$$

The waveform itself remains one-dimensional, whereas the associated blade labels and coefficients describe a sparse multivector. The application object can therefore be viewed at two levels: a grade-aware multivector and a relational architecture defined over its active grade sectors. If $\mathcal{M}^{(r)}$ denotes the active grade-r part, a generic inter-grade relation can be written abstractly as

$$\mathcal{R}_{rs} = \Phi_{rs}\Big(\mathcal{M}^{(r)}, \mathcal{M}^{(s)}\Big), \qquad r \neq s, \tag{6}$$

where Φ_{rs} is chosen for the application. Eq. (6) is deliberately general: it may represent a statistical coupling, geometric correspondence, graph relation, tensor contraction, conditional dependence, or another measurable relation. This separation keeps the GA blade semantics explicit without forcing every useful dependency to be an exterior product.

3. Encoding and Extraction FB-GA Algorithms

The transmitter and receiver perform conceptually different tasks. The encoder first constructs a labelled sparse multivector and then synthesizes a waveform. The extractor starts from the waveform and reconstructs only those blades whose complete address signatures satisfy the prescribed rules.

After extraction, a relational analyzer may operate on the accepted dictionary $\widehat{\mathcal{M}}$. The first decoding level answers which blades are present and estimates their coefficients. The second level asks how those accepted structures are organized with respect to one another. The final state descriptor may combine grade-specific coefficients with selected relational terms $\mathcal{R}_{rs}$.

Algorithm 1 Sparse FB-GA encoding.

Require: Sparse blade dictionary $\mathcal{M}$, coefficient envelopes $c_A(t)$, collision-free carrier map, phase reference, and orientation convention

Ensure: One real multiplexed signal $s_{\mathrm{FB-GA}}(t)$

1: Canonicalize every active blade label and record the permutation sign
2: Verify that no active blade repeats a basis direction
3: Assign one address to each grade-one blade, a paired address group to each bivector, and a prescribed multi-address group to each higher grade
4: Convert each complex coefficient into in-phase and quadrature envelopes relative to the common phase reference
5: For a requested higher grade, apply an explicit exterior-composition rule before signal synthesis
6: Multiply every envelope by the carriers assigned to its blade and apply the orientation sign as a coefficient sign or phase shift of π
7: Sum all grade-specific channels into one real waveform
8: Store the carrier map, blade labels, phase corrections, synthesis gains, and orientation metadata

Algorithm 2 Sparse FB-GA extraction.

Require: Received real signal, carrier map, phase corrections, synthesis gains, and blade convention

Ensure: Decoded sparse blade dictionary $\widehat{\mathcal{M}}$

1: Estimate the complex coefficient in every predefined narrow band by coherent demodulation, a short-time Fourier transform, or an equivalent method
2: Group the estimated channels according to their candidate blade labels
3: Reject groups that do not contain all required addresses or do not exceed the chosen detection threshold
4: Correct the deterministic carrier phases and orientation signs in each multi-address group
5: Compare the corrected coefficients within every candidate bivector, trivector, or higher-grade signature
6: Accept a blade only when its group satisfies the specified magnitude and phase-consistency conditions
7: Restore the canonical orientation and reconstruct the coefficient $\widehat{c}_A(t)$
8: Return accepted blades and classify rejected groups as unassigned spectral products

4. Illustrative Encoding Using Beijing Data

This section illustrates the encoder described above. It is not an environmental experiment and does not claim a physical relation among pollutants and meteorological variables. Measured data are used only because they provide nontrivial, naturally varying coefficient envelopes.

The input is the Dongsi station file from the Beijing Multi-Site Air Quality collection [5]. The complete collection contains hourly pollution and meteorological

measurements from twelve monitoring stations between March 2013 and February 2017. Three columns are retained and mapped to an abstract basis,

$$e_1 \leftrightarrow \mathrm{NO}_2, \qquad e_2 \leftrightarrow \mathrm{PM}_{2.5}, \qquad e_3 \leftrightarrow \mathrm{WSPM}. \tag{7}$$

Here NO_2 is nitrogen dioxide concentration in $\mu\mathrm{g\,m^{-3}}$, $\mathrm{PM}_{2.5}$ is the mass concentration of airborne particles with aerodynamic diameter not exceeding $2.5\,\mu$m, also in $\mu\mathrm{g\,m^{-3}}$, and WSPM is the source-data abbreviation for wind speed in $\mathrm{m\,s^{-1}}$. The mapping in Eq. (7) is a modelling convention. The atmospheric variables are not literal orthogonal spatial directions.

4.1 Preprocessing and Analytic Coefficients

Timestamps are reconstructed from the year, month, day, and hour columns. Missing values in the selected variables are filled by linear interpolation. Each complete series is standardized,

$$x_i(t) = \frac{X_i(t) - \mu_i}{\sigma_i}, \tag{8}$$

where $X_i(t)$ is the original series, μ_i its sample mean, and σ_i its population standard deviation. Standardization produces dimensionless envelopes with comparable scales. The selected interval is 28 November 2015 20:00 to 5 December 2015 19:00. The date has no inferential meaning.

Each standardized real series is converted to an analytic signal,

$$z_i(t) = x_i(t) + \mathrm{i}\mathcal{H}\{x_i(t)\}. \tag{9}$$

The Hilbert transform supplies an approximately 90°-shifted quadrature component. Thus $z_i(t)$ provides a local complex coefficient with amplitude $|z_i(t)|$ and phase $\arg z_i(t)$.

Fig. 1 displays the standardized envelopes.

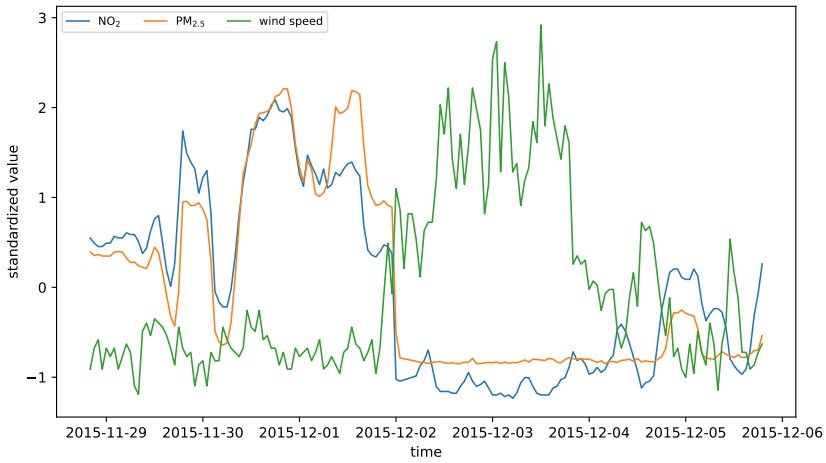

Fig. 1 *Standardized measured series used as coefficient envelopes.*

4.2 Two Sparse Objects and Oriented Pair Coefficients

Two illustrative objects are defined,

$$\mathcal{A}(t) = z_1(t)e_1 + z_2(t)e_2 + B_{12}(t)e_{12}, \tag{10}$$

$$\mathcal{B}(t) = z_2(t)e_2 + z_3(t)e_3 + B_{23}(t)e_{23}. \tag{11}$$

Object $\mathcal{A}$ contains two vector channels and their oriented pair relation. Object $\mathcal{B}$ shares e_2, adds e_3, and contains a second pair relation. Their blade-wise intersection is

$$\mathcal{A} \cap_{\text{blade}} \mathcal{B} = \{e_2\}. \tag{12}$$

Eq. (12) means only that e_2 is active in both sparse dictionaries.

The illustrative bivector coefficients are

$$B_{12}(t) = \mathrm{Im}\{z_1(t)z_2^*(t)\}, \qquad B_{23}(t) = \mathrm{Im}\{z_2(t)z_3^*(t)\}. \tag{13}$$

They encode oriented phase-plane relations. Their signs reverse if the order of the participating basis labels is exchanged.

4.3 Trivector as a Bivector–Vector Exterior Composition

The grade-three extension is formed from the already oriented e_{12} plane and the independent e_3 direction,

$$\big(B_{12}(t)e_{12}\big) \wedge \big(z_3(t)e_3\big) = T_{123}(t)e_{123}, \tag{14}$$

with

$$T_{123}(t) = B_{12}(t)z_3(t). \tag{15}$$

The coefficient is complex because $B_{12}(t)$ is real in this illustration while $z_3(t)$ carries the amplitude and phase of the third vector channel. Grade three is created by the explicit exterior composition in Eq. (14); it is not inferred from the numerical multiplication alone.

The full illustrative object is

$$\mathcal{C}(t) = z_1(t)e_1 + z_2(t)e_2 + z_3(t)e_3 + B_{12}(t)e_{12} + B_{23}(t)e_{23} + T_{123}(t)e_{123}. \tag{16}$$

Beyond this construction, an application may ask whether the bivector coefficient $B_{12}(t)$ is systematically related to the trivector coefficient $T_{123}(t)$, whether the vector component $z_3(t)$ modulates or predicts this relation, or whether changes in the vector sector are accompanied by reproducible reorganizations of the bivector and trivector sectors. These questions concern the relational organization of already identified GA structures and therefore represent a different level of analysis from the algebraic construction expressed by Eq. (15).

For a data-driven application, the joint pattern of active blades and selected inter-grade relations can be summarized as a *multigrade relational fingerprint*. Such a fingerprint need not have one universal mathematical form. It may contain, for example, normalized cross-grade similarities, phase-sensitive dependencies, conditional statistics, graph links, or tensor-derived correspondences. Its purpose is to retain information about how the grade-specific parts of a multivector participate in one state. Two observations can therefore be locally similar while having different multigrade relational fingerprints.

4.4 Collision-Free Frequency-Bin Synthesis

The measured hourly samples act as slowly varying envelopes. Each sample is repeated over a one-second synthetic carrier block sampled at 128 Hz. The carrier addresses in Tab. I were selected to avoid collisions within the displayed band.

Grade	Blade/signature	Address or addresses (Hz)
1	e_1, e_2, e_3	$5, 9, 15$
2	e_{12}	$4, 14$
2	e_{23}	$6, 24$
3	e_{123}	$1, 11, 19, 29$

Tab. I *Spectral addresses used by the illustrative FB-GA encoder.*

Let $\widetilde{B}_{12}(t)$, $\widetilde{B}_{23}(t)$, and $\widetilde{T}_{123}(t)$ denote optionally scaled synthesis coefficients. This scaling is used only to keep the illustrative waveform within a convenient dynamic range. The multiplexed real waveform is

$$\begin{aligned} s(t) = {} & \mathrm{Re}\{z_1(t)\mathrm{e}^{\mathrm{i}2\pi 5t}\} + \mathrm{Re}\{z_2(t)\mathrm{e}^{\mathrm{i}2\pi 9t}\} + \mathrm{Re}\{z_3(t)\mathrm{e}^{\mathrm{i}2\pi 15t}\} \\ & + 0.45\widetilde{B}_{12}(t)\,[\cos(2\pi 4t) + \cos(2\pi 14t)] \\ & + 0.45\widetilde{B}_{23}(t)\,[\cos(2\pi 6t) + \cos(2\pi 24t)] \\ & + 0.25\sum_{r=1}^{4} \mathrm{Re}\Big\{\alpha_r \widetilde{T}_{123}(t)\mathrm{e}^{\mathrm{i}2\pi f_{123,r}t}\Big\}, \end{aligned} \tag{17}$$

where $(f_{123,1}, f_{123,2}, f_{123,3}, f_{123,4}) = (1, 11, 19, 29)$ Hz and $(\alpha_1, \alpha_2, \alpha_3, \alpha_4) = (1, 1, 1, -1)$. The factors α_r form a deterministic address-specific sign code used only by the illustrative synthesizer. They are known to the decoder and removed before the four channels are compared; they are distinct from the GA orientation factor η_{ijk}. The constants 0.45 and 0.25 are visualization gains. Blade identity is determined by the address group and metadata, not by these gains.

Fig. 2 shows a short excerpt of the resulting waveform. Fig. 3 shows its spectrum. Because time-varying envelopes generate sidebands around the nominal spectral

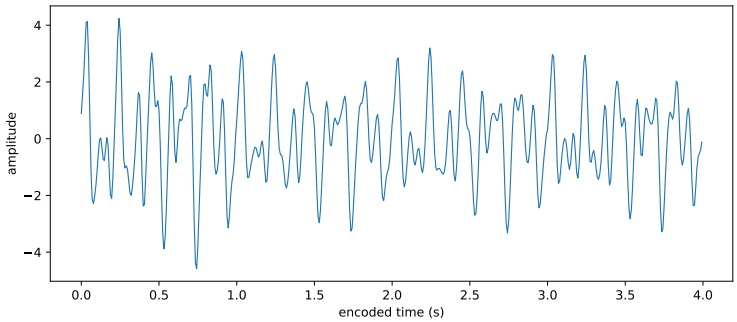

Fig. 2 *Short excerpt of one real waveform that multiplexes grade-one, grade-two, and grade-three coefficient channels.*

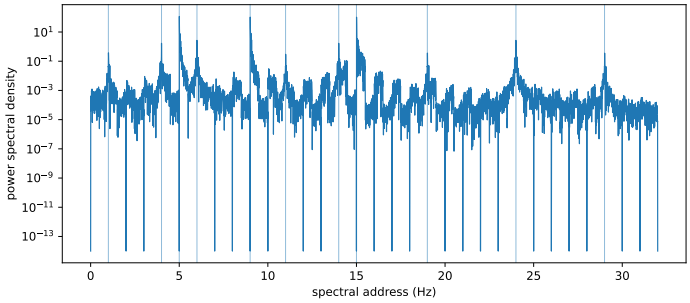

Fig. 3 *Spectrum of the illustrative multiplexed signal. The vertical locations correspond to the predefined address map; peaks alone do not establish blade identity.*

addresses, the complex coefficients should be estimated over predefined narrow frequency bands rather than extracted from a single Fourier bin.

The example demonstrates how a single signal can carry elementary components, higher-grade structures, and relational information. After successful blade reconstruction, the decoded vector, bivector, and trivector can also be analysed jointly to form a multigrade relational fingerprint. In a validated sensing application, such a fingerprint could serve as a compact descriptor for recognizing system states, detecting anomalies, comparing distributed systems, or tracking structural transitions over time.

5. Frequency-Bin Quantum-Like Informatics

FB-GA also provides a signal-domain language for frequency-bin quantum-like systems. The qualifier *quantum-like* is deliberate. Classical signal processors can reproduce superposition, interference, controlled mixing, and non-factorizable coefficient patterns, but these operations do not by themselves establish microscopic quantumness, Bell nonlocality, or quantum computational advantage [6–8].

5.1 Frequency-Bin q-Bits and q-Dits

A normalized two-state object is

$$|\psi\rangle = \alpha|0\rangle + \beta|1\rangle, \qquad |\alpha|^2 + |\beta|^2 = 1. \tag{18}$$

The complex amplitudes α and β determine the relative weights and phases of the logical states. A frequency-bin analogue assigns the two states to two orthogonal spectral modes,

$$\Psi(f) = \alpha\delta_{\mathrm{D}}(f - f_0) + \beta\delta_{\mathrm{D}}(f - f_1), \tag{19}$$

where δ_{D} is the Dirac distribution and f_0, f_1 are distinct state addresses. A corresponding real waveform is the real part of $\alpha e^{i2\pi f_0 t} + \beta e^{i2\pi f_1 t}$. More than two bins define a q-dit-like signal representation.

Consider two subsystems, each with two states,

$$|\psi_A\rangle = \alpha|0\rangle_A + \beta|1\rangle_A, \qquad |\psi_B\rangle = \gamma|0\rangle_B + d|1\rangle_B. \tag{20}$$

The symbol d is used for the second complex amplitude of subsystem B so that it cannot be confused with the Dirac distribution δ_{D}. Their frequency-domain representations are

$$\Psi_A(f) = \alpha\delta_{\mathrm{D}}(f - f_{A0}) + \beta\delta_{\mathrm{D}}(f - f_{A1}), \tag{21}$$
$$\Psi_B(f) = \gamma\delta_{\mathrm{D}}(f - f_{B0}) + d\delta_{\mathrm{D}}(f - f_{B1}). \tag{22}$$

Convolution of the two spectra corresponds to multiplication of the corresponding signals in the time domain and can be expressed as

$$\begin{aligned}\Psi_{AB}(f) &= (\Psi_A * \Psi_B)(f) \\ &= \alpha\gamma\,\delta_{\mathrm{D}}(f - f_{A0} - f_{B0}) + \alpha d\,\delta_{\mathrm{D}}(f - f_{A0} - f_{B1}) \\ &\quad + \beta\gamma\,\delta_{\mathrm{D}}(f - f_{A1} - f_{B0}) + \beta d\,\delta_{\mathrm{D}}(f - f_{A1} - f_{B1}).\end{aligned} \tag{23}$$

Eq. (23) is the frequency-bin counterpart of the Kronecker composition

$$|\psi_{AB}\rangle = \alpha\gamma|00\rangle + \alpha d|01\rangle + \beta\gamma|10\rangle + \beta d|11\rangle. \tag{24}$$

The first term of Eq. (23) represents joint state $|00\rangle$ at address $f_{A0} + f_{B0}$. The second represents $|01\rangle$, the third $|10\rangle$, and the fourth $|11\rangle$. The products $\alpha\gamma$, αd, $\beta\gamma$, and βd are exactly the Kronecker-product coefficients of the local amplitude vectors. If the corresponding time-domain waveform is required to be real, conjugate negative-frequency components must also be included to satisfy Hermitian symmetry.

5.2 Controlled Convolution and Separability

A physical mixer generally produces all spectral products allowed by the underlying signal interaction. FB-GA introduces an additional rule layer that selects only those channels consistent with the intended composite object, assigns the corresponding blade labels, and preserves the required orientation and phase information. We refer to this constrained operation as *controlled convolution*. It should be distinguished both from the projective-geometric-algebra join and from unconstrained spectral convolution.

Let the joint coefficients be arranged in a matrix

$$A = \begin{bmatrix} a_{00} & a_{01} \\ a_{10} & a_{11} \end{bmatrix}. \tag{25}$$

The state is separable when there exist local coefficient vectors u and v such that $A = uv^{\mathsf{T}}$. If no such factorization exists, the classical waveform has an entanglement-like correlation structure. In a genuine single-photon frequency-bin implementation, related transformations can have physical quantum meaning [9–11].

Programmable frequency-bin processors can perform mixing, phase shifts, and unitary transformations and may therefore support classical emulation and photonic prototyping of small q-bit and q-dit circuits, while retaining an explicit relation between hardware channels and labelled algebraic objects.

5.3 Polarization-Selective Controlled Convolution

The complex modes

$$p_R(f,t) = \mathrm{e}^{+\mathrm{i}2\pi ft}, \qquad p_L(f,t) = \mathrm{e}^{-\mathrm{i}2\pi ft} \tag{26}$$

rotate in opposite directions in the complex plane. They are labelled right-rotating (R) and left-rotating (L) modes. A detector that observes only $|f|$ may lose this handedness, whereas an I/Q-sensitive or polarization-sensitive detector can preserve it.

Frequency polarization and GA blade orientation are related but conceptually distinct. Polarization is a property of the complex mode or physical field. Blade orientation is an algebraic sign convention associated with the ordering of basis directions. An implementation may map one to the other, but the mapping must be stated explicitly.

Two polarized two-state subsystems generate four candidate joint labels,

$$RR, \quad RL, \quad LR, \quad LL. \tag{27}$$

A polarization-selective controlled convolution can be designed to retain only equal-handed channels RR and LL and to reject RL and LR. When the accepted channels have equal magnitudes and a fixed relative phase ϕ, the coefficient pattern is

$$|\Phi_{\mathrm{FB}}\rangle = \frac{1}{\sqrt{2}}\left(|RR\rangle + \mathrm{e}^{\mathrm{i}\phi}|LL\rangle\right). \tag{28}$$

Two locations may separately report identical magnitude spectra because a detector resolves only $|f|$. Their local observations can therefore appear equal even when one contains right-rotating and the other left-rotating modes. A joint I/Q-sensitive measurement reveals the hidden polarization relation. Depending on the relative phase, some mixed channels interfere destructively while others reinforce.

Chiral and anisotropic media can transform right- and left-handed modes differently [12]. Comparing input and output FB-GA objects may therefore provide a structured description of how a medium changes elementary bins, polarization, and relational signatures. More generally, this example illustrates an application principle: locally similar or even identical lower-grade observations can correspond to different higher-order or inter-grade relational structures.

6. FB-GA for Neural and Cognitive Modelling

Neural activity is commonly analysed through oscillatory bands, cross-frequency coupling, phase-amplitude interactions, and large-scale coherence [13–15]. FB-GA suggests a broader possibility: a perceptual or cognitive state may be represented not only by local spectral components, but by the *relational geometry* formed jointly by distributed complex neural modes. The question is therefore not whether a frequency or anatomical location is active, but whether the organization among multiple modes is reproducible and informative.

Let a prospective neural representation be a complex field

$$z_c(k,t) = A_c(k,t)e^{\mathrm{i}\phi_c(k,t)}, \tag{29}$$

where c denotes a perceptual condition, k a spectral, graph-spectral, spatial, or other selected mode, and t time. Rather than assigning identity to one coefficient, two contents may be compared through the geometry of their fields. A natural distance is

$$D(c,c') = \sum_{k,t} |z_c - z_{c'}|^2 = \sum_{k,t} \left[(A_c - A_{c'})^2 + 2A_cA_{c'}\big(1 - \cos(\phi_c - \phi_{c'})\big)\right]. \tag{30}$$

The decomposition shows that two states may have similar local spectral amplitudes but differ in how their phases are organized across the system. The relevant information may therefore lie in a reproducible pattern of relations rather than in any single oscillation or anatomical location.

Writing the neural multivector schematically as

$$\mathcal{M}_c(k,t) = \sum_{r=0}^{m} \mathcal{M}_c^{(r)}(k,t), \tag{31}$$

one may associate selected inter-grade maps

$$\mathcal{R}_{rs}^{(c)} = \Phi_{rs}\Big(\mathcal{M}_c^{(r)}, \mathcal{M}_c^{(s)}\Big), \qquad r \neq s, \tag{32}$$

with each condition. The collection of stable grade-specific structures and inter-grade maps constitutes a candidate multigrade relational fingerprint. The operator Φ_{rs} is not fixed by FB-GA alone; it must be chosen according to the experimental question and validated against appropriate null models and competing descriptors.

A percept may also be an *ensemble* object rather than an exact single-trial invariant. Repeated realizations could converge toward a stable geometry,

$$\mathcal{G}_c^{(n)} \longrightarrow \mathcal{G}_c^{*} \qquad (n \to \infty), \tag{33}$$

while individual realizations remain variable.

Spatiotemporal Geometry Integration Theory (SGIT) is a prospective research programme that uses the FB-GA representation as one possible mathematical language for studying how distributed dynamical components become organized into reproducible integrated structures. The term *spatiotemporal* emphasizes that the relevant object is not restricted to temporal frequency bins: spatial, graph-spectral, anatomical, or other distributed modes can be combined with temporal evolution in a common representation. SGIT therefore concerns the geometry of organization across both space and time rather than a static spectrum alone.

A future mathematical direction for SGIT is *Spatiotemporal Multigrade Relational Geometry*. In this viewpoint, a state is described by three complementary levels: the spatiotemporal modes themselves, the grade-specific geometric structures constructed from those modes, and the relations among structures belonging to different grades. The third level is essential because two states may contain comparable lower-order components while differing in how pairwise, triple, and higher-order structures are mutually coordinated.

A practical SGIT research sequence is therefore to identify reproducible spatiotemporal geometry across runs or subjects, separate amplitude-dominated from phase-sensitive structure, test whether individual grade sectors add information beyond conventional descriptors, and then test whether inter-grade maps $\mathcal{R}_{rs}$ provide additional reproducible information beyond the constituent sectors. Seen/unseen paradigms, matched-stimulus controls, perturbation experiments, and independent replication can then ask whether particular multigrade relational invariants track conscious access rather than stimulus energy or generic neural activity.

FB-GA therefore need not claim that the brain literally executes geometric-algebra algorithms or that a multivector is consciousness. Its useful role is to provide a unified language in which local components, oriented pair relations, higher-order structures, inter-grade relations, and candidate invariants can be formulated as separate, falsifiable hypotheses. This perspective is compatible with geometric-algebra approaches to integrated information [18] and with information-physics models of complex systems [19, 20]. It offers a possible formal route toward the neural binding problem [17]: the identity of a percept may reside partly in a reproducible geometry of relations that is not reducible to a list of independently active components.

7. Conclusion

From an engineering viewpoint, FB-GA trades bandwidth, calibration effort, and metadata for explicit interpretability. Multi-address signatures use additional spectral resources, the carrier plan must avoid collisions, and coherent complex estimation is required. In return, the receiver can reconstruct a labelled object whose components encode grade, orientation, and relational role. Tensor descriptions can store similar multi-index information directly in software, while FB-GA is particularly useful when a signal-level realization, physical carrier architecture, or explicit mapping between carrier and relational semantics is part of the design.

The Beijing example is intentionally non-inferential. Its purpose is to demonstrate that measured, nonstationary signals can be transformed into complex coefficients, organized into labelled vector, bivector, and trivector structures, and multiplexed without carrier collisions. Once reconstructed, the same FB-GA object can support a second analytical layer in which relations among different grade sectors are examined as a multigrade relational fingerprint. In a validated sensing application, such a fingerprint could provide a compact descriptor for comparing system states, detecting anomalies, and tracking transitions in the underlying relational structure.

In quantum-like information processing, frequency-bin hardware provides a natural carrier space for controlled composition, interference, polarization-sensitive selection, and non-factorizable coefficient structures. FB-GA can add explicit grade and relational labels to these operations while keeping classical emulation conceptually separate from genuine quantum claims.

In neural and cognitive applications, the same representation offers a path from local oscillatory components toward reproducible spatiotemporal and multigrade relational descriptions, which SGIT can develop in dedicated experimental studies. Oscillatory components, oriented pair relations, selected higher-order coordination

patterns, and inter-grade dependencies can be represented within one explicit framework. Validation must still compare the resulting structures with established coherence, higher-order spectral, state-space, graph, and causal methods, while controlling for common-reference effects, nonstationarity, and multiple testing [13–16].

Acknowledgement

This work was supported by the European Union under the project Robotics and Advanced Industrial Production (No. CZ.02.01.01/00/22_008/0004590) and by the Slovak Grant Agency VEGA (No. 1/0779/25).

References

[1] LU H.-H., LUKENS J.M., PETERS N.A., ODELE O.D., LEAIRD D.E., WEINER A.M., LOUGOVSKI P.: Electro-optic frequency beam splitters and tritters for high-fidelity photonic quantum information processing, *Physical Review Letters*, 2018, 120, 030502, doi: 10.1103/PhysRevLett.120.030502.

[2] LUKENS J.M., LOUGOVSKI P.: Frequency-encoded photonic qubits for scalable quantum information processing, *Optica*, 2017, 4(1), pp. 8–16, doi: 10.1364/OPTICA.4.000008.

[3] DORAN C., LASENBY A.: *Geometric Algebra for Physicists*. Cambridge: Cambridge University Press, 2003.

[4] LAVOR C., XAMBÓ-DESCAMPS S., ZAPLANA I.: *A Geometric Algebra Invitation to Space-Time Physics, Robotics and Molecular Geometry*. Cham: Springer, 2018, doi: 10.1007/978-3-319-90665-2.

[5] CHEN S.: Beijing Multi-Site Air Quality, UCI Machine Learning Repository, 2017, doi: 10.24432/C5RK5G.

[6] KHRENNIKOV A.: *Ubiquitous Quantum Structure: From Psychology to Finance*. Berlin: Springer, 2010, doi: 10.1007/978-3-642-05101-2.

[7] HAVEN E., KHRENNIKOV A.: *Quantum Social Science*. Cambridge: Cambridge University Press, 2013, doi: 10.1017/CBO9781139003664.

[8] SVÍTEK M., KOSHELEVA O., KREINOVICH V., NGUYEN T.N.: Why quantum (wave probability) models are a good description of many non-quantum complex systems, and how to go beyond quantum models. In: *Studies in Computational Intelligence*, 2019, 809, pp. 168–175.

[9] LU H.-H., SIMMERMAN E.M., LOUGOVSKI P., WEINER A.M., LUKENS J.M.: Fully arbitrary control of frequency-bin qubits in a quantum frequency processor, *Physical Review Letters*, 2020, 125, 120503, doi: 10.1103/PhysRevLett.125.120503.

[10] LU H.-H., LUKENS J.M., WILLIAMS B.P.: A controlled-NOT gate for frequency-bin qubits, *npj Quantum Information*, 2019, 5, 24, doi: 10.1038/s41534-019-0137-z.

[11] LU H.-H., KLCO N., LUKENS J.M.: Simulations of subatomic many-body physics on a quantum frequency processor, *Physical Review A*, 2019, 100, 012320, doi: 10.1103/PhysRevA.100.012320.

[12] CRIMIN F., MACKINNON N., GÖTTE J.B., BARNETT S.M.: Optical helicity and chirality: conservation and sources, *Applied Sciences*, 2019, 9, 828, doi: 10.3390/app9050828.

[13] CANOLTY R.T., KNIGHT R.T.: The functional role of cross-frequency coupling, *Trends in Cognitive Sciences*, 2010, 14, 11, pp. 506–515, doi: 10.1016/j.tics.2010.09.001.

[14] HYAFIL A., GIRAUD A.-L., FONTOLAN L., GUTKIN B.: Neural cross-frequency coupling: connecting architectures, mechanisms, and functions, *Trends in Neurosciences*, 2015, 38, 11, pp. 725–740, doi: 10.1016/j.tins.2015.09.001.

[15] FRIES P.: Rhythms for cognition: communication through coherence, *Neuron*, 2015, 88, 1, pp. 220–235, doi: 10.1016/j.neuron.2015.09.034.

[16] KOVACH C.K., OYA H., KAWASAKI H.: The bispectrum and its relationship to phase-amplitude coupling, *NeuroImage*, 2018, 173, pp. 518–539, doi: 10.1016/j.neuroimage.2018.02.033.

[17] FELDMAN J.: The neural binding problem(s), *Cognitive Neurodynamics*, 2013, 7, 1, pp. 1–11, doi: 10.1007/s11571-012-9219-8.

[18] SVÍTEK M.: Integrated information assessment using geometric algebra, *Neural Network World*, 2024, 34, 3, pp. 189–201, doi: 10.14311/NNW.2024.34.010.

[19] SVÍTEK M.: *Information Physics: Physics-Information and Quantum Analogies for Complex Systems Modeling*. Academic Press, 2021.

[20] SVÍTEK M.: Emergent intelligence in generalized pure quantum systems, *Computation*, 2022, 10, 6, 88, doi: 10.3390/computation10060088.

[21] SVÍTEK M.: Frequency-Bin Geometric Algebra for Structured and Relational Information: Theoretical Foundations, *Neural Network World*, 2026, 36, 3, doi: 10.14311/NNW.2026.36.003.